Chinese Journal of Natural Medicines

Isodons AH, *seco*–abietane and abietane–type diterpenoids from *Isodon lophanthoides*: isolation, structural elucidation, and anti–cholestatic activity

Huiling Zhou, Mingzhu Han, Miaomiao Nan, Yingrong Leng, Weiming Huang, Shengtao Ye, Lingyi Kong, Wenjun Xu, Hao Zhang

Citation: Huiling Zhou, Mingzhu Han, Miaomiao Nan, Yingrong Leng, Weiming Huang, Shengtao Ye, Lingyi Kong, Wenjun Xu, Hao Zhang, Isodons AH, *seco*–abietane and abietane–type diterpenoids from *Isodon lophanthoides*: isolation, structural elucidation, and anti–cholestatic activity, Chinese Journal of Natural Medicines, 2025, 23(9), 1133–1142. doi: 10.1016/S1875–5364(25)60977–0.

View online: https://doi.org/10.1016/S1875–5364(25)60977–0

Chinese Journal of Natural Medicines 23 (2025) 1133-1142

Contents lists available at ScienceDirect

Chinese Journal of Natural Medicines

journal homepage: www.cjnmcpu.com/

Original article

Isodons A–H, *seco*-abietane and abietane-type diterpenoids from *Isodon lophanthoides*: isolation, structural elucidation, and anti-cholestatic activity

Huiling Zhou, Mingzhu Han, Miaomiao Nan, Yingrong Leng, Weiming Huang, Shengtao Ye, Lingyi Kong*, Wenjun Xu*, Hao Zhang*

State Key Laboratory of Natural Medicines, Joint International Research Laboratory of Target Discovery and New Drug Innovation (Ministry of Education), School of Traditional Chinese Pharmacy, Affiliated Jiangning Chinese Medicine Hospital, China Pharmaceutical University, Nanjing 210009, China

ARTICLE INFO

Article history:
Received 21 July 2024
Revised 3 November 2024
Accepted 9 November 2024
Available online 20 September 2025

Keywords:
Isodon lophanthoides
Diterpenoids
Anticholestatic effect
FXR
Cyp7a1

ABSTRACT

Eight new diterpenoids, Isodons A–H (**1**–**8**), comprising *seco*-abietane and abietane-type structures, together with 13 known analogues (**9**–**21**), were isolated from *Isodon lophanthoides* (Buch.-Ham. ex D. Don) Hara. The compounds (+)-**3**/(−)-**3**, (+)-**4**/(−)-**4**, and (+)-**5**/(−)-**5** were identified as three enantiomeric pairs. The planar structures and absolute configurations of **1**–**8** were determined through high-resolution electrospray ionization mass spectrometry (HR-ESI-MS), 1D & 2D nuclear magnetic resonance (NMR) spectroscopy, electronic circular dichroism (ECD) calculations, and X-ray diffraction crystallography. A cholesterol 7α-hydroxylase (Cyp7a1) luciferase reporter assay revealed significant anti-cholestatic activities for compounds **1**, (+)-**4**, **6**, **7**, **12**–**14**, and **16**. Additionally, compound **6** demonstrated anti-cholestatic effects through the farnesoid X receptor (FXR)-associated signaling pathways *in vitro* and *in vivo*. These findings suggest potential applications for *I. Lophanthoides* in pharmaceutical development.

1. Introduction

Cholestasis is a significant clinical liver disease characterized by impaired bile formation, secretion, and flow [1]. Without appropriate treatment, cholestasis may progress to liver fibrosis, cirrhosis, or liver failure [2,3]. Present treatment options for cholestasis are limited to ursodeoxycholic acid (UDCA) and obeticholic acid (OCA) [4]. These medications, however, demonstrate variable efficacy among patients and may induce serious adverse effects [5]. The exploration of natural products for novel therapeutic agents remains an active area of research [6]. Traditional Chinese medicine has extensively utilized various herbs for treating dampness and jaundice. *Isodon lophanthoides* (Buch.-Ham. ex D. Don) Hara, known as 'Xihuangcao' in China, is a perennial herb [7]. This species grows predominantly in swamps and forested areas across China, India, Thailand, Vietnam, Myanmar, and Bhutan [7]. In China's Lingnan region, 'Xihuangcao' serves as a traditional medicine recognized for its hepatoprotective properties. The herb demonstrates clinical efficacy in treating conditions including acute icterohepatitis, hepatitis B virus infection, cholecystitis, and enteritis [8]. 'Xihuangcao' tea is consumed as a health-promoting beverage [7,9], and its soup preparation maintains popularity in China [10]. *I. Lophanthoides* is classified within the genus *Isodon* of the Lamiaceae family [11]. The genus *Isodon* encompasses approximately 150 species globally [12]. Phytochemical analyses have identified diterpenoids as the primary active components of the genus *Isodon* [13]. Besides ent-kauranes, abietanes and ent-abietanes represent the predominant diterpenoids in *Isodon* species [12]. Diterpenoids isolated from *I. Lophanthoides* have garnered significant interest due to their structural complexity and diverse biological activities. While current research on *I. Lophanthoides*-derived diterpenoids has primarily focused on anti-inflammatory, anti-tumor, anti-biotic, and anti-viral properties; studies examining their anti-cholestatic potential remain limited. Therefore, investigating the characteristic diterpenoid constituents and anti-cholestatic activity of *I. Lophanthoides* holds substantial importance. Comprehensive phytochemical and biological analyses of these diterpenoids will facilitate the development and utilization of *I. Lophanthoides*.

This investigation details the isolation and structural determination of 24 compounds, comprising 5 previously undescribed compounds and 3 pairs of novel enantiomers. Their planar structures and absolute configurations were established through high-resolution electrospray ionization mass spectrometry (HR-ESI-MS), 1D & 2D nuclear magnetic resonance (NMR), electronic circular dichroism (ECD) analyses, and single crystal X-ray diffraction. Luciferase reporter assay revealed that most compounds demonstrated inhibitory effects on cholesterol 7α-hydroxylase (Cyp7a1) promoter luciferase activity. Notably, compound **6** demonstrated efficacy in alleviating α-naphthylisothiocyanate (ANIT)-induced bile acid accumulation, liver injury, and inflammation *in vivo*. Additional molecular studies indicated that com-

* Corresponding author.
E-mail addresses: cpu_lykong@126.com (L. Kong); wjxu@cpu.edu.cn (W. Xu); zhanghao@cpu.edu.cn (H. Zhang)

https://doi.org/10.1016/S1875-5364(25)60977-0

pound **6** achieved its anti-cholestatic effect *via* regulation of liver farnesoid X receptor (FXR)-associated pathways *in vitro* and *in vivo*.

2. Results and Discussion

Isodon A (**1**) was isolated as colorless bulk crystals with a molecular formula of $C_{20}H_{26}O_4$, determined from the HR-ESI-MS ion peak at *m/z* 353.1729 $[M + Na]^+$ (Calcd. for $C_{20}H_{26}NaO_4$, 353.1723) indicating eight degrees of unsaturation. The ^{13}C NMR spectrum displayed twenty carbon resonances, with ten arising from the aromatic carbons of the naphthalene ring (C-5-C-14, Table 1) (rings B and C, Fig. 1). The heteronuclear multiple bond correlation (HMBC) (Fig. 2) from Me-20 to C-5, C-6, and C-10, from OH-12 to C-11, C-12, and C-13, and from the geminal Me-16 and Me-17 to C-13 and C-15 (δ_C 73.0) demonstrated the presence of C-5 methyl, C-12 hydroxy, and C-13 2-hydroxypropan-2-yl moieties, respectively. The long-range HMBC of H-1/C-2, C-3, C-9, of Me-18/C-3, and of Me-19/C-4, combined with the ^1H–^1H correlation spectroscopy (COSY) interactions of H-1/H_2-2/H_2-3 (Fig. 2) confirmed a 2,2-dimethyloxocan-5-ol moiety (ring A) fused at the naphthalene ring (C-9, C-10, C-11) in **1**. The ^4J correlations from Me-18 to C-11 in its HMBC spectrum (Fig. S2–4) further verified the C-4-O-C-11 linkage. The absolute configuration of **1** was determined as 1*R* through single-crystal diffraction experiment using Cu Kα radiation with a Flack parameter of −0.10(7) (Fig. 3). Consequently, **1** was characterized as a *seco*-abietane type diterpenoid and designated as isodon A.

Table 1 ^1H and ^{13}C NMR spectroscopic data for **1** and **2**.

No.	**1**[a,b]		**2**[a,b]	
	δ_H, mult. (*J*, Hz)	δ_C	δ_H, mult. (*J*, Hz)	δ_C
1	5.52, dd (11.9, 6.4)	69.3	3.92, td (13.6, 5.3)	26.5
			2.93, m	
2	2.43, m	30.3	2.18, m	23.1
	2.0, m		1.67, m	
3	1.39, dt (15.9, 3.7)	34.6	1.24, dt (15.3, 3.5)	33.5
	1.56, m		1.58, dt (15.3, 3.5)	
4		84.9		85.6
5		133.3		133.6
6	7.10, d (8.3)	127.3	7.12, d (8.2)	127.4
7	7.54, d (8.3)	128.4	7.49, d (8.2)	126.6
8		128.2		127.6
9		128.4		130.5
10		132.1		131.9
11		132.5		135.4
12		147.8		146.7
13		133.8		133.7
14	7.48, s	122.4	7.46, s	120.7
15		73.0		72.8
16	1.59, s	29.6	1.70, s	29.6
17	1.70, s	29.2	1.74, s	29.4
18	1.19, s	25.9	1.16, s	27.6
19	1.73, s	26.1	1.64, s	26.6
20	2.48, s	21.2	2.44, s	20.0
12-OH			6.92, s	

[a]: ^1H NMR data calculated in 600 MHz in $CDCl_3$ (δ in ppm, *J* in Hz); [b]: ^{13}C NMR data calculated in 150 MHz in $CDCl_3$.

Isodon B (**2**) was isolated as yellow bulk crystals. The molecular formula of **2** was determined as $C_{20}H_{26}O_3$, 16 mass units less than **1**, based on the HR-ESI-MS ion peak at *m/z* 337.1785 $[M + Na]^+$ (Calcd. for $C_{20}H_{26}NaO_3$, 337.1774). Comparative analysis of the 1D NMR data indicated that **2** shared the same core skeleton with **1** (Table 1). The primary distinction was the absence of C-1 oxy-methine resonances in **2** compared to **1**. This structural feature was confirmed by the HMBC from H_2-1 to C-2, C-3, and C-10, and the ^1H–^1H COSY interactions of H_2-1/H_2-3/H_2-4 (Fig. 2). Single-crystal diffraction analysis Cu Kα radiation further substantiated this structural determination (Fig. 3). Therefore, **2** was characterized as shown and named isodon B (Fig. 1).

Isodon C (**3**) was isolated as colorless bulk crystals. Its molecular formula was determined to be $C_{20}H_{24}O_4$ based on the HR-ESI-MS ion peak at at *m/z* 351.1568 $[M + Na]^+$ (Calcd. for $C_{20}H_{24}NaO_4$, 351.1567). The 1D NMR data (Table 2) revealed the same 13-(2-hydroxypropan-2-yl)-5-methyl-naphthalene-11,12-diol fragment as **1** and **2**. This structural determination was confirmed by the heteronuclear single quantum correlation (HSQC) and HMBC data of **3**. The ^1H–^1H COSY of H-1/H-2 and the HMBC from H-1 to C-5, C-9, and C-10, and from H-2 to C-1, C-10, and C-11 (Fig. 2) established a pyran-like ring (ring A) fused at the C-9, C-10, and C-11 of the naphthalene ring (rings B and C). The C-1 hydroxy and C-2 2-methylprop-1-en-1-yl substituents at ring A were established by the HMBC (Fig. 2) from the olefinic H-3 to C-1 (δ_C 67.3), C-2, and C-4, and from Me-18 and Me-19 to C-3 and C-4. X-ray crystallographic diffraction analysis (Fig. 3) revealed that **3** existed as a racemic mixture with the relative configuration of H-1α and H-2β. Chiral high performance liquid chromatography (HPLC) separation of **3** produced a pair of enantiomers, (+)-**3** and (−)-**3**, in an approximate ratio of 1∶1 (Fig. S1). The absolute configurations of (+)-**3** and (−)-**3** were confirmed through ECD calculations. The correspondence between the calculated ECD curve of (1*S*,2*R*)-**3** and the experimental ECD curve of (−)-**3** (Fig. 4) established the absolute configuration of (+)-**3** and (−)-**3** as 1*R*,2*S* and 1*S*,2*R*, respectively. The structure of compound (+)-**3**/(−)-**3**, designated as (+)-isodon C/(−)-isodon C, was conclusively determined.

Isodon D (**4**) was isolated as a brown powder. Its molecular formula was determined to be $C_{20}H_{22}O_4$ based on the HR-ESI-MS ion peak *m/z* 349.1423 $[M + Na]^+$ (Calcd. for $C_{20}H_{22}NaO_4$, 349.1410), differing from **3** by 2 mass units. Detailed analysis of the 1D NMR spectroscopic data (Table 2) of **4** and **3** indicated structural similarity. The key difference was the presence of a C-1 carbonyl group in **4**, replacing the C-1 hydroxyl group found in **3**. The degrees of unsaturation of **4** as indicated by its HR-ESI-MS spectrum (Fig. S5–6) and the HMBC (Fig. 2) from H-2, H-3, and Me-20 to C-1 (δ_C 193.1) confirmed the C-1 carbonyl group. The negligible optical value and absence of significant ECD Cotton effects indicated that compound **4** was also a racemic mixture. (+)-**4** and (−)-**4** were obtained through chiral HPLC separation of **4**; the absolute configurations of (+)-**4** and (−)-**4** were determined as 2*R* and 2*S*, respectively, through comparison of experimental and calculated ECD spectra (Fig. 4). Thus, the structure of (+)-**4**/(−)-**4** was established as shown in Fig. 1 and designated as (+)-isodon D/(−)-isodon D.

Isodon E (**5**) was isolated as a brown powder. The molecular formula of $C_{20}H_{24}O_4$, identical to that of **3**, was determined by the detection of an ion peak at *m/z* 351.1571 $[M + Na]^+$ (Calcd. for $C_{20}H_{24}NaO_4$, 351.1567) in the HR-ESI-MS spectrum of **5**. The structural distinction between **5** and **3** was attributed to the position of the double bond ($\Delta^{4,18}$ in **5**, $\Delta^{3,4}$ in **3**). This assignment was substantiated by the HMBC (Fig. 2) from the olefinic H_2-18 to C-3, C-4, C-19, from Me-19 to C-3, C-4, C-18, and from H_2-3 to C-1 and

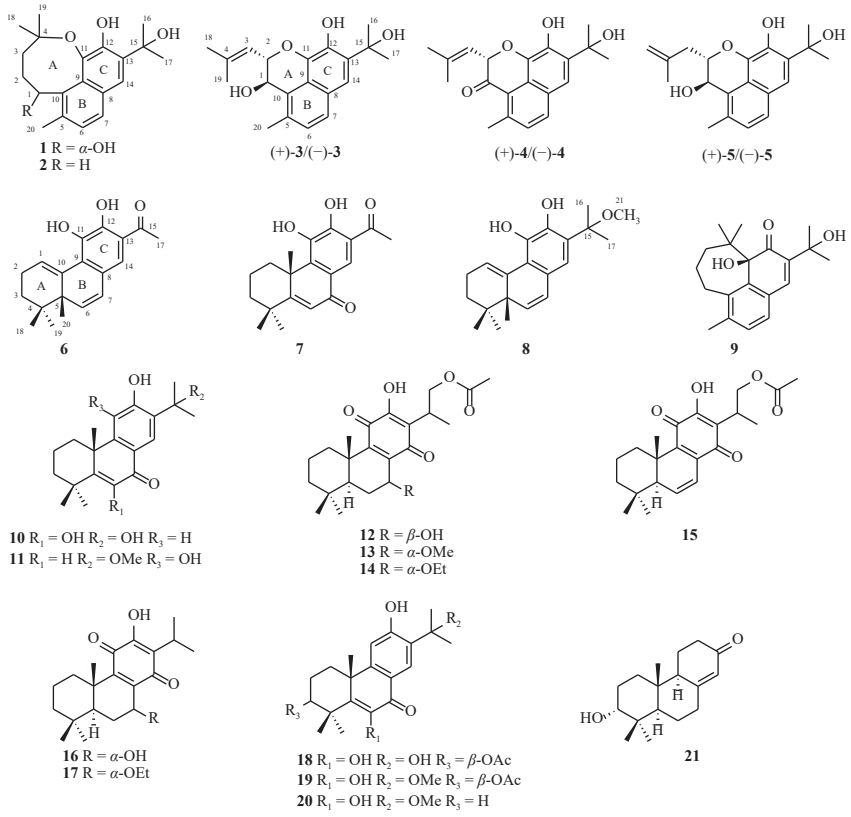

Fig. 1 Structures of compounds **1**–**21**.

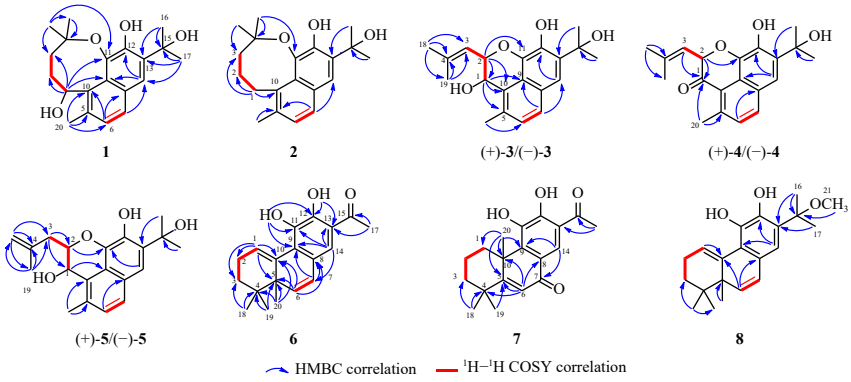

Fig. 2 Key COSY and HMBC correlations of compounds **1**–**8**.

C-2. Chiral HPLC resolution of **5** yielded two optically pure enantiomers, (+)-**5** and (−)-**5**, in an approximate ratio of 1∶1 (Fig. S1).

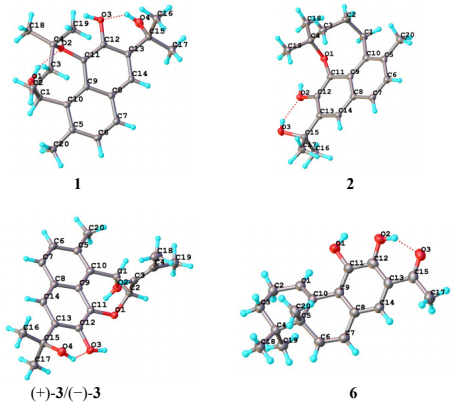

Fig. 3 X-ray crystallographic structures of **1**, **2**, (+)-**3**/(−)-**3**, and **6**.

The ECD curves of (+)-**5** and (+)-**3** (Fig. 4) exhibited nearly identical patterns, indicating shared absolute configurations of 1*R*,2*S*. ECD calculations further confirmed the absolute configurations of (+)-**5** and (−)-**5**. Consequently, the structure of (+)-**5**/(−)-**5** was established as shown in Fig. 1, designated as (+)-isodon E/(−)-isodon E.

Isodon F (**6**) was obtained as yellow bulk crystals. Its molecular formula, $C_{19}H_{22}O_3$, was determined by the HR-ESI-MS ion peak at *m/z* 321.1466, $[M + Na]^+$ (Calcd. for $C_{19}H_{22}NaO_3$, 321.1461), indicating nine degrees of unsaturation. Compound **6** was identified as a C-16-nor-abietane-type diterpenoid based on 1D NMR resonances (with HSQC experiment assistance). The $^1H–^1H$ COSY cross-peaks of H-1/H_2-2, H_2-2/H_2-3 and the HMBC (Fig. 2) from an olefinic H-1 to C-2, C-3, C-5, C-10, from the geminal Me-18 and Me-19 to C-3, C-4, C-5, and from Me-20 to C-4, C-5, C-10 confirmed ring A in the structure of **6** (Fig. 1). The characteristic coupling constant of an endocyclic double bond ($J_{H\text{-}6,H\text{-}7}$ = 9.8 Hz) (Table 3) and the HMBC (Fig. 2) from these two olefinic hydrogens (H-6 and H-7) to C-5, C-8, C-9, C-10, and from Me-20

Table 2 ^{1}H and ^{13}C NMR spectroscopic data for **3** and **4**.

No.	**3**[b, d]		**4**[a, c]	
	δ_H, mult. (*J*, Hz)	δ_C	δ_H, mult. (*J*, Hz)	δ_C
1	4.91, d (2.0)	67.3		193.1
2	5.40, dd (8.8, 2.0)	77.9	5.47, d (8.7)	79.9
3	4.85, m	120.1	5.34, m	118.7
4		139.7		141.9
5		133.7		140.8
6	7.20, d (8.4)	127.6	7.23, d (8.4)	128.9
7	7.64, d (8.4)	128.3	7.86, d (8.4)	134.2
8		126.1		126.0
9		120.0		123.5
10		124.8		120.5
11		134.2		134.6
12		140.0		141.8
13		134.9		135.3
14	7.33, s	116.0	7.42, s	117.1
15		73.9		74.1
16	1.73, s	30.1	1.78, s	30.0
17	1.76, s	29.7	1.77, s	29.8
18	1.86, d (1.4)	18.9	1.88, d (1.4)	19.1
19	1.59, d (1.4)	25.9	1.76, s	26.1
20	2.54, s	18.0	2.80, s	22.4

[a]: ^{1}H NMR data calculated in 600 MHz in $CDCl_3$; [b]: ^{1}H NMR data calculated in 500 MHz in $CDCl_3$ (*J* in Hz); [c]: ^{13}C NMR data calculated in 150 MHz in $CDCl_3$; [d]: ^{13}C NMR data calculated in 125 MHz in $CDCl_3$.

to C-5, C-6, C-10 established ring B (Fig. 1). The HMBC (Fig. 2) from the aromatic H-14 to C-7-C-9 and C-11-C-13, and from the OH-11 and OH-12 to C-9 and C-11-C-13 confirmed the aromatized ring C (Fig. 1). The C-13 acetyl group was verified by the HMBC (Fig. 2) of Me-17 to C-13 and C-15 (δ_C 204.2). The absolute configuration of **6** was determined as 5*S* through X-ray crystallographic analysis with a Flack parameter of −0.11(10) (Fig. 3). Thus, the structure of **6**, named isodon F, was established (Fig. 1).

Isodon G (**7**) was isolated as a yellow powder. The HR-ESI-MS ion peak at *m/z* 337.1417, $[M + Na]^+$ (Calcd. for $C_{19}H_{22}NaO_3$, 337.1410) established a molecular formula of $C_{19}H_{22}O_3$ for **7**, indicating nine degrees of unsaturation. The characteristic resonances of the geminal Me-18 and Me-19, the angular methyl group (Me-20), the aromatized ring C, and the C-13 acetyl group were evidenced by the ^{1}H and ^{1}C NMR data of **7** (Table 4). In comparison with the 1D NMR data of **6** (Table 3), the analysis revealed the absence of the endocyclic double bond ($\Delta^{6,7}$) in **6** and the presence of a conjugated α,β-unsaturated carbonyl [δ_C 175.4 (C-5), 123.5 (C-6), 184.6 (C-7)] moiety in **7**. The HMBC (Fig. 2) from the olefinic H-6 to C-4, C-5, C-8, C-10, from Me-20 to C-1, C-5, C-9, C-10, from the geminal Me-18 and Me-19 to C-3, C-4, C-5 and from the aromatic H-14 to C-7 confirmed the α,β-unsaturated carbonyl fused ring B and the migrated angular methyl group from C-5 (in **6**) to C-10 (in **7**). This structural determination aligned with the molecular formula of **7** and the ^{1}H-^{1}H COSY cross-peaks (Fig. 2) of H_2-1/H_2-2 and H_2-2/H_2-3 in **7**. The significantly deshielded ^{13}C NMR resonances (Table 4) of C-5 (δ_C 175.4) resulted from the conjugation effect of the C-7 ketone and the aromatized ring C [7, 14]. The 10*S* configuration of **7** was confirmed through comparison between the experimental and calculated ECD curves of (10*S*)-**7** (Fig. 4). Consequently, the structure of **7** was established and designated as isodon G.

Isodon H (**8**) was isolated as a yellow powder. The molecular formula of **8** was established as $C_{21}H_{28}O_3$ based on the ion peak at *m/z* 351.1936, $[M + Na]^+$ (Calcd. for $C_{21}H_{28}NaO_3$, 321.1461), in its HR-ESI-MS spectrum. Compound **8** exhibited 1D NMR spectroscopic data similar to those of **6** (Table 3 and Table 4), with the notable difference being the presence of a 2-methoxypropan-2-yl moiety in **8** rather than the C-13 acetyl group in **6**. This structural feature was supported by the HMBC (Fig. 2) from the geminal Me-16 and Me-17 to C-13 and C-15, and from the methoxy Me-21 to C-15. The absolute configuration of **8** was determined as 5*R* through comparison of the calculated ECD spectrum of 5*R*-**8** with the experimental ECD spectrum of **8** (Fig. 4). Therefore, the structure of **8** was established as shown in Fig. 1 and designated as isodon H.

Through comparison of 1D NMR and HR-ESI-MS data of the 13 known compounds with corresponding literature data, the following compounds were identified: wulfenioidin G (**9**) [15], 6,12,15-trihydroxy-5,8,11,13-abietetriene-7-one (**10**) [16], gerardianin C (**11**) [14], gerardianin B (**12**) [14], 16-acetoxy-7a-methoxyro-yleanone (**13**) [17], 16-acetoxy-7a-ethoxyroyleanone (**14**) [18], micranthin B (**15**) [19], horminone (**16**) [20], 7α-ethoxyroyleanone (**17**) [21], graciliflorin F (**18**) [7], 15-*O*-methylgraciliflorin F (**19**) [7], graciliflorin E

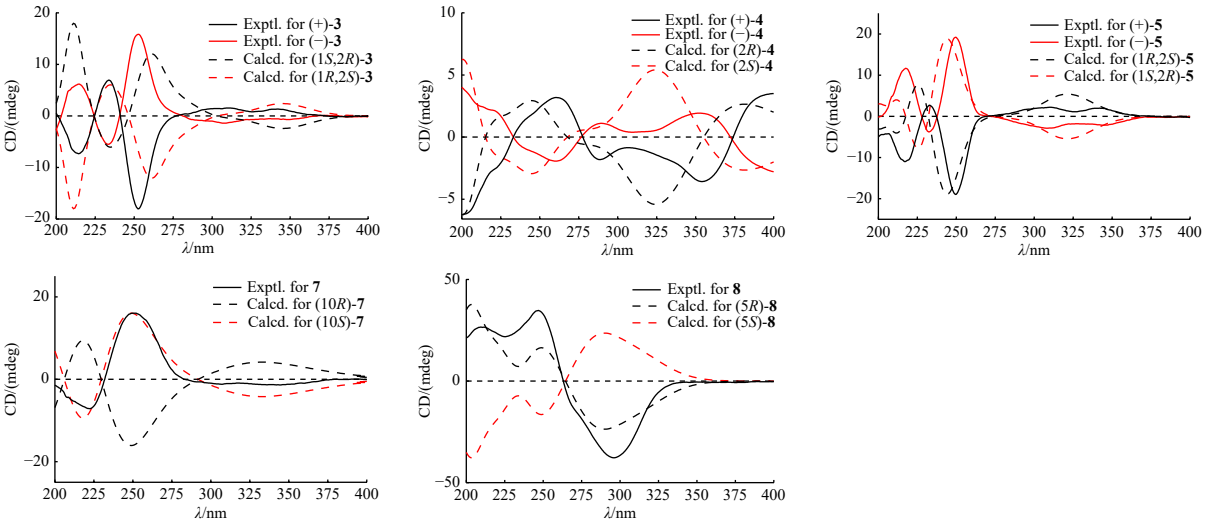

Fig. 4 Experimental and computational ECD spectra of compounds **3**, **4**, **5**, **7**, and **8**.

Table 3 ^{1}H and ^{13}C NMR spectroscopic data for **5** and **6**.

No.	**5**[a, b]		**6**[a, b]	
	δ_H, mult. (*J*, Hz)	δ_C	δ_H, mult. (*J*, Hz)	δ_C
1	4.89, d (1.7)	66.3	6.82, d (4.2)	132.2
2	4.81, ddd (8.3, 6.2, 1.7)	78.7	2.30, m	24.0
			2.30, m	
3	2.05, m	39.2	1.29, m	32.3
	1.92, m		1.92, m	
4		141.1		33.3
5		133.8		42.5
6	7.12, d (8.4)	127.6	5.96, dd (9.8, 1.6)	134.2
7	7.57, d (8.4)	128.3	6.24, dd (9.8, 1.6)	124.1
8		126.0		125.0
9		119.9		126.0
10		124.2		134.3
11		133.3		143.0
12		140.0		149.7
13		135.1		116.7
14	7.26, s	116.1	6.91, s	118.2
15		73.9		204.2
16	1.65, s	29.7		
17	1.67, s	29.8	2.59, brs	26.5
18	4.75, m	113.9	1.04, s	25.0
	4.41, m			
19	1.75, s	22.5	0.95, s	25.0
20	2.47, s	17.9	1.07, s	23.2

[a]: ^{1}H NMR data calculated in 600 MHz in $CDCl_3$ (*J* in Hz); *b*: ^{13}C NMR data calculated in 150 MHz in $CDCl_3$.

(**20**) [7], and graciliflorin B (**21**) [11].

2.1. Biological activities

The incidence of cholestasis has shown a steady increase in recent years. Current surgical and pharmacological interventions demonstrate limited efficacy across all patients and present significant adverse effects on healthy tissues [4]. Therefore, the development of novel therapeutic agents for cholestasis treatment represents an urgent medical need.

FXR plays a crucial role in bile acid homeostasis and cholestasis prevention through its regulation of bile acid synthesis, detoxification, and transport [22]. In hepatic tissue, FXR activation promotes the transcription of transporter genes facilitating bile acid clearance, including *Mrp2* and *Bsep*, and genes involved in bile acid uptake such as *Oatp-1* and *Ntcp*, while suppressing genes associated with bile acid biosynthesis, including *Cyp7a1* and *Cyp8b1* [4]. Therefore, FXR is thought to be an important target for treating cholestasis.

Cyp7a1 functions as the rate-limiting enzyme in the classical pathway of bile acid synthesis [23]. This enzyme facilitates cholesterol conversion to bile acids and maintains lipid homeostasis [23]. In our investigation of compounds with potential therapeutic effects on cholestatic liver injury, we established a screening model based on Cyp7a1 promoter luciferase activity. Initially, we

Table 4 ^{1}H and ^{13}C NMR spectroscopic data for **7** and **8**.

No.	**7**[a, b]		**8**[a, b]	
	δ_H, mult. (*J*, Hz)	δ_C	δ_H, mult. (*J*, Hz)	δ_C
1	3.34, m	33.9	6.65, t (4.0)	128.4
	1.42, m			
2	1.98, m	18.7	2.30, m	23.8
	1.64, m		1.08, d (2.2)	
3	1.74, m	40.4	1.93, m	32.5
	1.46, m		1.27, m	
4		38.4		33.3
5		175.4		42.7
6	6.49, s	123.5	5.88, d (9.8)	133.3
7		184.6	6.18, d (9.8)	124.8
8		122.7		125.4
9		143.6		119.2
10		42.8		134.7
11		142.0		143.0
12		152.1		142.1
13		117.9		126.0
14	8.29, s	120.7	6.27, s	115.5
15		205.6		80.3
16			1.59, s	26.5
17	2.72, s	26.8	1.56, s	26.2
18	1.37, s	29.7	1.03, s	25.1
	1.28, s			
19		33.2	0.96, s	25.1
20	1.68, s	24.7	1.09, s	22.9
21			3.23, s	51.0

[a]: ^{1}H NMR data calculated in 500 MHz in $CDCl_3$ (*J* in Hz); [b]: ^{13}C NMR data calculated in 125 MHz in $CDCl_3$.

evaluated the cytotoxicity of 21 compounds in AML12 cells using the cell counting kit-8 (CCK8) assay, as shown in Table 5. Subsequently, to assess the impact of these compounds on Cyp7a1 expression, we conducted a luciferase reporter assay in HepG2 cells *via* transient transfection with FXR target gene Cyp7a1 promoter reporter vector. The results indicated that compounds **1**, (+)-**4**, **6**, **7**, **12**–**14**, and **16** demonstrated significant inhibitory effects on Cyp7a1 promoter luciferase activity (Fig. 5). Based on quantity, toxicity, and activity profiles of candidate compounds, compound **6** was selected for subsequent *in vitro* and *in vivo* studies.

2.2. Effects of compound **6** on the FXR and downstream effectors in cells

To investigate the effect of compound **6** on FXR expression, the FXR protein expression was evaluated in mouse hepatocytes AML12 cells and human hepatocytes L02 cells. AML12 and L02 cells were treated with 1, 2, and 4 μmol·L^{-1} of **6**, respectively (Figs. 6A and 6B). The results demonstrated that **6** significantly enhanced FXR protein expression while reducing Cyp7a1 protein expression, suggesting that **6** stimulated FXR expression and

Table 5 IC_{50} values of compounds **1**–**21** in AML12 cells.

Compounds	IC_{50} (μmol·L^{-1})	Compounds	IC_{50} (μmol·L^{-1})
1	> 100	**10**	97.61 ± 0.32
2	83.87 ± 2.24	**11**	48.52 ± 0.04
(+)-**3**	>100	**12**	20.43 ± 1.69
(−)-**3**	> 100	**13**	> 100
(+)-**4**	>100	**14**	65.49 ± 0.81
(−)-**4**	> 100	**15**	42.76 ± 0.80
(+)-**5**	> 100	**16**	23.35 ± 0.53
(−)-**5**	> 100	**17**	> 100
6	98.92 ± 1.18	**18**	85.39 ± 0.38
7	108.77 ± 2.04	**19**	46.93 ± 1.26
8	74.05 ± 0.51	**20**	47.16 ± 0.96
9	83.40 ± 1.27	**21**	> 100

transcriptionally suppressed Cyp7a1 expression. Additionally, **6** increased the messenger ribonucleic acid (mRNA) expression of *OST-β* and *Bsep*, while inhibiting the mRNA expression of *Cyp7a1*, which are established FXR downstream target genes (Fig. 6C). These findings indicated that **6** activated the FXR pathway.

*2.3. Effects of compound **6** on ANIT-induced cholestasis and liver injury*

To evaluate the anti-cholestatic effect of **6**, an ANIT-induced mouse model of cholestasis and liver injury was utilized. C57BL/6J mice received oral administration of corn oil, ANIT, UDCA, or compound **6**. A single dose of ANIT at 80 mg·kg^{-1} induced edema, hepatic necrosis, inflammatory cell infiltration, hepatic collagen deposition and fibrosis. These pathological changes were significantly reduced following six days of **6** or UDCA administration (Fig. 7B). Serum ALT and AST levels serve as sensitive indicators of liver function impairment, while ALP and TBA function as biochemical indicators of biliary toxicity [1, 24]. These biochemical markers were elevated after ANIT administration compared to the control group (Fig. 7C). Treatment with compound **6** or UDCA substantially reduced these elevations. These results demonstrated that **6** provided protection against ANIT-induced hepatotoxicity and cholestasis.

*2.4. Effects of compound **6** on the FXR and inflammatory factors in ANIT-induced mouse model*

To further validate the effect of compound **6** on FXR expression, we examined the protein expression in the livers of ANIT-induced mouse model. The results demonstrated that **6** enhanced the protein level of FXR compared with the ANIT group (Fig. 8A). The downstream *Cyp7a1* mRNA level decreased following **6** administration (Fig. 8B). Additionally, we analyzed the expression of inflammatory factors using the quantitative reverse transcription-polymerase chain reaction (qRT-PCR) method. ANIT elevated the expressions of *Tnf-α*, *Il-6*, and *Il-1β*, whereas compound **6** or UDCA treatment significantly suppressed the inflammatory factors expression (Fig. 8C). These findings indicated that compound **6** exhibited hepatoprotective effects through FXR activation and inflammatory response reduction *in vivo*.

3. Conclusions

In summary, 8 new *seco*-abietane and abietane diterpenoids, along with 13 known compounds were isolated from dried whole *I. Lophanthoides* in this study. Compounds **1**, (+)-**4**, **6**, **7**, **12**–**14**, and **16** demonstrated significant inhibitory effects in Cyp7a1 luciferase reporter assay. Further investigation revealed that compound **6** protected against ANIT-induced cholestatic liver injury in mice through activation of the FXR signaling pathway, potentially affecting bile acid synthesis, detoxification and transportation. These findings provide a scientific basis for the use of *I. Lophanthoides* as hepatoprotective agents.

4. Experimental

4.1. General experimental procedures

Optical rotations, UV, ECD, and IR spectra of compounds were measured using a JASCO P-1020 polarimeter, a Shimadzu UV-2450 UV/vis spectrophotometer, a JASCO J-810 spectrometer, and a Bruker Tensor-27 infrared spectrometer with KBr disks, respectively. HR-ESI-MS data was acquired from an Agilent 6520B UPLC-Q-TOF instrument. NMR data were recorded and obtained on a Bruker AV-500/600 NMR instrument, using TMS as an internal standard. Preparative HPLC was performed with an Agilent 1100 series instrument using an Agilent ZORBAX SB-C_{18} column (10 μm, 250 mm × 21.2 mm, i.d.). The HPLC analysis was conducted on an Agilent 1100 series system with an Agilent ZORBAX Eclipse XDB-C_{18} column (5 μm, 4.6 mm × 150 mm, i.d.). Column chromatography was performed using silica gel (100–200 mesh and 200–300 mesh; Qingdao Haiyang Chemical Co., Ltd., Qingdao, China), ODS RP-C_{18} (40–63 μm, Fuji, Japan) and MCI (Mitsubishi, Japan). Enantiomers were separated using Phenomenex Cellulose-2 chiral preparative column (5 μm, 250 mm × 21.2 mm, i.d.).

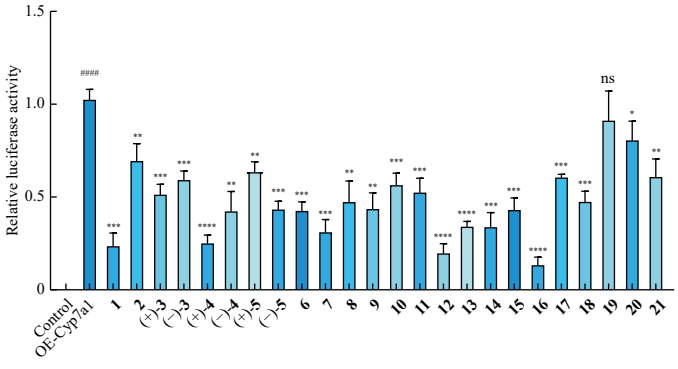

Fig. 5 Effects of compounds **1**–**21** (10 μmol·L^{-1}) on Cyp7a1 promoter luciferase activitiy. Data are shown as the mean ± SD (n = 3). $^{\#\#\#\#}P < 0.0001$ *vs* Control; $^{*}P < 0.05$, $^{**}P < 0.01$, $^{***}P < 0.001$, and $^{****}P < 0.0001$ *vs* OE-Cyp7a1 group.

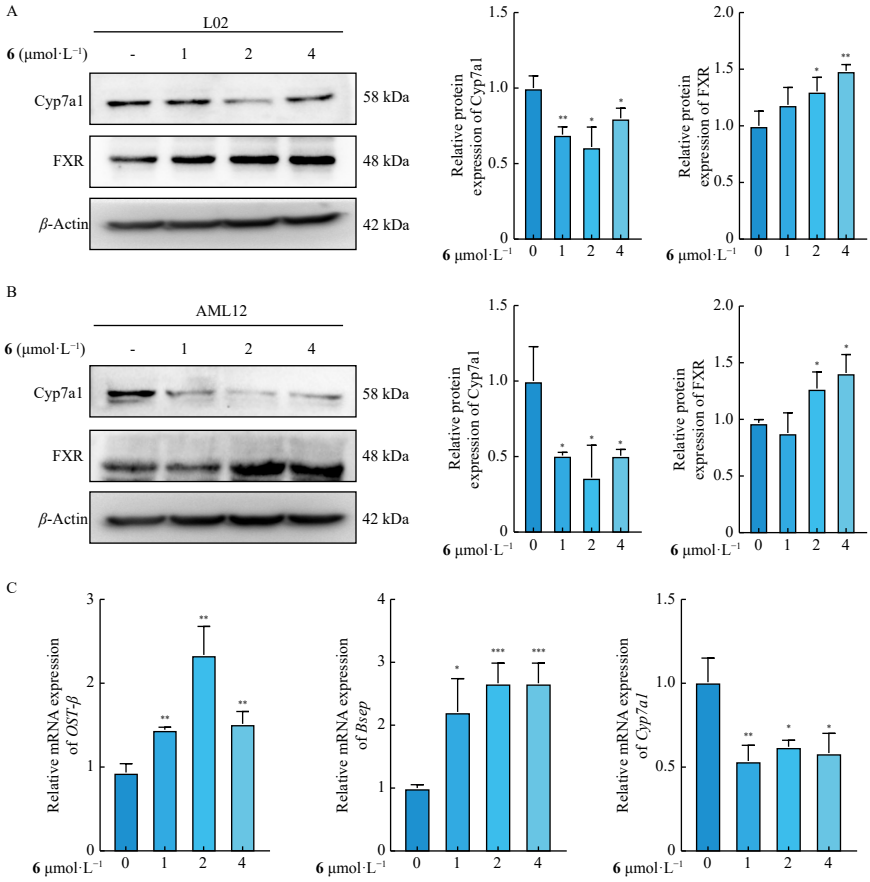

Fig. 6 Effect of **6** on the expression of FXR and Cyp7a1 in human hepatocytes L02 cells and FXR, Cyp7a1, OST-β, and Bsep in mouse hepatocytes AML12 cells. (A) The protein levels of FXR and Cyp7a1 in L02 cells were evaluated by Western blot. (B) The protein levels of FXR and Cyp7a1 in AML12 cells were evaluated by Western blot. (C) The mRNA levels of *Ost-β*, *Bsep*, and *Cyp7a1* were detected by qRT-PCR in AML12 cells. Data are shown as the mean ± SD (n = 3). $^{*}P < 0.05$, $^{**}P < 0.01$, $^{***}P < 0.001$ *vs* DMSO group.

4.2. Plant material

The whole plants of *I. Lophanthoides* were purchased from Guangdong Province in August 2022. A voucher specimen (No. 2020-ILMH) was deposited in the Department of Natural Medicinal Chemistry and verified by Professor Guoyong Xie from China Pharmaceutical University.

4.3. Extraction and isolation

The dried and powdered whole herbs of *I. Lophanthoides* (20 kg) were extracted with 95% EtOH three times under reflux heating. The extracted solution was concentrated under vacuum to yeild 2.5 kg of brown extract, which was dissolved in distilled water and partitioned with petroleum ether (PE). The PE-soluble fraction (472.7 g) was chromatographed on a silica gel column using a gradient of PE–EtOAc (from 50∶1 to 1∶1, *V*/*V*) to obtain six fractions (1–6). Fr. 1 (60 g) was subjected to silica gel chromatography with PE–DCM (from 1∶0 to 0∶1, *V*/*V*) to yield seven further fractions (1A–1F). Fr. 1D (600 mg) was purified by preparative HPLC (MeOH–H_2O, 88∶12, 10 mL·min^{-1}) to afford **6** (120 mg, t_R = 19.9 min) and **17** (80 mg, t_R = 26.9 min). Fr. 1F (1 g) was processed by preparative HPLC (MeOH–H_2O, 84∶16, 10 mL·min^{-1}) to yield **5** (10 mg, t_R = 35 min). Fr. 2 (24.7 g) was chromatographed on an ODS gel column with MeOH–H_2O (from 60∶40 to 100∶0, *V*/*V*) to obtain eight subfractions (2A–2H). Compounds **9** (80 mg, t_R = 10 min) and **15** (80 mg, t_R = 17 min) were isolated from Fr. 2B (2.5 g) by preparative HPLC (MeOH–H_2O, 76∶24, 10 mL·min^{-1}). Compound **8** (20 mg, t_R = 30 min) was obtained from Fr. 2F (428 mg) by preparative HPLC (MeOH–H_2O, 75∶25, 10 mL·min^{-1}). Fr. 3 (51.1 g) was subjected to MCI gel chromatography with MeOH–H_2O (from 60∶40 to 100∶0, *V*/*V*) to yield 6 subfractions (3A–3F). Fr. 3D (1.8 g) was purified by preparative HPLC (ACN–H_2O, 80∶20, 10 mL·min^{-1}) to obtain compounds **2** (20 mg, t_R = 10 min) and **14** (70 mg, t_R = 15 min). Fr. 3E (2.4 g) was separated by silica gel column with PE–EtOAc (from 15∶1 to 0∶1, *V*/*V*) and purified using an ODS column (MeOH–H_2O, 66∶34) to obtain compounds **10** (72 mg), **11** (90 mg) and **3** (10 mg). Fr. 4 (29.8 g) was fractionated on an MCI gel column with MeOH–H_2O (from 70∶30 to 100∶0, *V*/*V*) and further purified by preparative HPLC (MeOH–H_2O, 78∶22, 10 mL·min^{-1}) to yield compounds **4** (10 mg, t_R = 10 min), **19** (6 mg, t_R = 25 min) and **12** (50 mg, t_R = 38 min). Fr. 5 (42.8 g) was chromatographed on an MCI gel column with MeOH–H_2O (from 42∶58 to 100∶0, *V*/*V*) to obtain four fractions (5A–5D). Fr. 5A (1.8 g) was purified by preparative HPLC (MeOH–H_2O, 65∶35, 10 mL·min^{-1}) to yield compound **20** (100 mg, t_R = 20 min). Fr. 5C (557 mg) was purified by ODS gel chromatography with MeOH–H_2O (60∶40 to 100∶0, *V*/*V*) to obtain compound **7** (20 mg). Fr. 6 (41.1 g) was separated on an MCI gel column with MeOH–H_2O (from 49∶51 to 100∶0, *V*/*V*), yielding four fractions (6A–6D). Compound **21** (18.6 mg, t_R = 20 min) was isolated from Fr. 6B (372 mg) by preparative HPLC (MeOH–H_2O, 65∶35, 10 mL·min^{-1}). Fr. 6C (4.8 g) was chromatographed on an ODS column with MeOH–H_2O (from 49∶51 to 100∶0, *V*/*V*) and purified by preparative HPLC (MeOH–H_2O, 60∶40, 10 mL·min^{-1}), yielding compounds **18** (20 mg, t_R = 10 min), **16** (30 mg, t_R = 16 min), **1** (5 mg, t_R = 23 min), and **13** (65 mg, t_R = 27 min). (+)-**4** (4 mg, t_R = 30 min) and (−)-**4** (4 mg, t_R = 38 min) were isolated from compound **4** using a Phenomenex Cellulose-2 chiral preparative column with (MeOH–H_2O, 78∶22, 10 mL·min^{-1}). The HPLC separation of compounds **3** and **5** was applied to the Phenomenex Cellulose-2 chiral preparative column with (MeOH–H_2O, 68∶32, 10 mL·min^{-1}) to give (+)-**3** (5 mg, t_R = 20 min) and (−)-**3** (5 mg, t_R = 24 min), (+)-**5** (3 mg, t_R = 30 min)

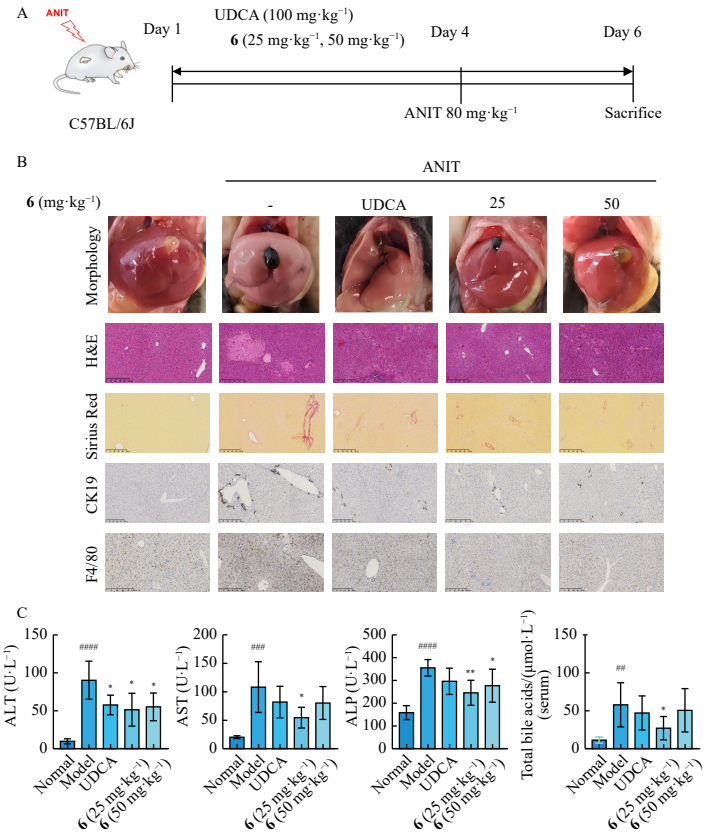

Fig. 7 Effect of **6** on cholestatic liver injury caused by ANIT. (A) The animal experimental scheme. (B) Morphology of mouse livers (top); H&E and IHC staining for CK19, F4/80, and Sirius Red in liver tissues (bottom). Scale Bar = 250 μm. (C) The levels of ALT, AST, ALP, and TBA in the serum samples. Data are shown as the mean ± SD (n = 6). $^{\#\#}P < 0.01$, $^{\#\#\#}P < 0.001$, $^{\#\#\#\#}P < 0.0001$ *vs* Normal; $^{*}P < 0.05$, $^{**}P < 0.01$, $^{***}P < 0.001$ *vs* Model.

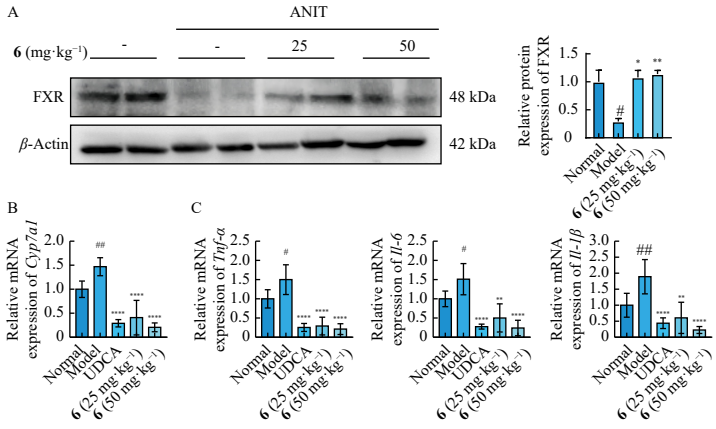

Fig. 8 Effect of **6** on the levels of FXR, Cyp7a1 and inflammatory genes in ANIT-treated mice. (A) The protein levels of FXR were detected by Western blotting. (B) The mRNA levels of *Cyp7a1* were detected by qRT-PCR. (C) The mRNA levels of inflammatory factors *Tnf-α*, *Il-1β*, and *Il-6* were detected by qRT-PCR. Data are shown as the mean ± SD (n = 6). $^{\#}P < 0.05$, $^{\#\#}P < 0.01$, $^{\#\#\#\#}P < 0.001$ *vs* Normal; $^{**}P < 0.01$, $^{***}P < 0.001$, $^{****}P < 0.0001$ *vs* Model.

and (−)-**5** (3 mg, t_R = 35 min), respectively.

Isodon A (***1***). Colorless bulk crystals; $[\alpha]_D^{25}$ −99.2 (*c* 0.106, MeOH); UV (MeOH) λ_{max} (log ε) 238.4 (4.34), 261.6 (3.46); ECD (MeOH) λ_{max}: 220.5 (+16.60), 237 (+4.37), 247 (+21.38), 336 (−10.15); IR (KBr) ν_{max}: 3363, 2938, 2920, 1625, 1382, 1368, 1175, 1005 cm^{-1}; ^1H (600 MHz, $CDCl_3$) and ^{13}C NMR (150 MHz, $CDCl_3$), see Table 1; HR-ESI-MS *m/z* 353.1729 $[M + Na]^+$, (Calcd. for $C_{20}H_{26}NaO_4$, 353.1723).

Isodon B (***2***). Yellow bulk crystals; $[\alpha]_D^{25}$ +5.8 (*c* 0.096, MeOH); UV (MeOH) λ_{max} (log ε) 238.8 (4.08), 261.4 (2.81); IR (KBr) ν_{max}: 3441, 2964, 2921, 1641, 1631, 1383, 1116, 789 cm^{-1}; ^1H (600 MHz, $CDCl_3$) and ^{13}C NMR (150 MHz, $CDCl_3$), see Table 1, HR-ESI-MS *m/z* 337.1785 $[M + Na]^+$, (Calcd. for $C_{20}H_{26}NaO_3$, 337.1774).

Isodon C (***3***). Colorless bulk crystals; (+)-**3**: $[\alpha]_D^{25}$ −44.9 (*c* 0.24, MeOH); ECD (MeOH) λ_{max} 214 (−7.27), 234 (6.93), 252.5 (−18.01); (−)-**3**: $[\alpha]_D^{25}$ +44.1 (*c* 0.24, MeOH); ECD (MeOH) λ_{max} 213.5 (6.09), 234 (−5.45), 252 (15.79); UV (MeOH) λ_{max} (log ε) 243.8 (4.28), 272.8 (3.35); IR (KBr) ν_{max}: 3397, 2926, 2926, 1658, 1649, 1370, 1190 cm^{-1}; ^1H (500 MHz, $CDCl_3$) and ^{13}C NMR (125 MHz, $CDCl_3$), see Table 2; HR-ESI-MS *m/z* 351.1568 $[M + Na]^+$, (Calcd. for $C_{20}H_{24}NaO_4$, 351.1567).

Isodon D (***4***). Brown powder; (+)-**4**: $[\alpha]_D^{25}$ +28.9 (*c* 0.11, MeOH); ECD (MeOH) λ_{max} 261.5 (3.17), 286.5 (−1.74), 308.5 (−0.86), 355 (−3.57); (−)-**4**: $[\alpha]_D^{25}$ −14.3 (*c* 0.07, MeOH); ECD (MeOH) λ_{max} 261.5 (−1.93), 288 (+1.09), 318 (+0.44), 354 (1.92); UV (MeOH) λ_{max} (log ε) 210.6 (4.29); IR (KBr) ν_{max}: 3397, 2925,

2853, 1659, 1365, 1189, 1026 cm^{-1}; ^1H (600 MHz, $CDCl_3$) and ^{13}C NMR (150 MHz, $CDCl_3$), see Table 2, HR-ESI-MS *m/z* 349.1423 $[M + Na]^+$, (Calcd. for $C_{20}H_{22}NaO_4$, 349.1410).

*Isodon E (**5**).* Brown powder; (+)-**5**: $[\alpha]_D^{25}$ −646.3 (*c* 0.10, ACN); ECD (MeOH) λ_{max} 217 (−10.99), 233.5 (+2.62), 249 (−18.80); (−)-**5**: $[\alpha]_D^{25}$ +497.0 (*c* 0.09, ACN); ECD (MeOH) λ_{max} 216.5 (+11.43), 232.5 (−3.76), 250.5 (+18.99); UV (MeOH) λ_{max} (log ε) 210.8 (4.25); IR (KBr) ν_{max}: 3422, 2965, 2926, 1658, 1642, 1383, 1195, 1019 cm^{-1}; ^1H (600 MHz, $CDCl_3$) and ^{13}C NMR (150 MHz, $CDCl_3$), see Table 3, HR-ESI-MS *m/z* 351.1571 $[M + Na]^+$, (Calcd. for $C_{20}H_{24}NaO_4$, 351.1567).

*Isodon F (**6**).* Yellow bulk crystals; $[\alpha]_D^{25}$ −491.4 (*c* 0.093, MeOH); UV (MeOH) λ_{max} (log ε) 332.4 (3.86), 296.0 (3.4), 266.2 (4.23), 212.2 (3.76); ECD (MeOH) λ_{max} 229.5 (+29.10), 326 (−37.35); IR (KBr) ν_{max}: 3475, 2964, 2918, 1622, 1307, 954 cm^{-1}; ^1H (600 MHz, $CDCl_3$) and ^{13}C NMR (150 MHz, $CDCl_3$), see Table 3, HR-ESI-MS *m/z* 321.1466 $[M + Na]^+$, (Calcd. for $C_{19}H_{22}NaO_3$, 321.1461).

*Isodon G (**7**).*Yellow powder; $[\alpha]_D^{25}$ −1.2 (*c* 0.104, MeOH); UV (MeOH) λ_{max} (log ε) 260.6 (4.14), 301.8 (3.36); ECD (MeOH) λ_{max} 221.5 (−6.92), 250.5 (+15.98), 336 (−1.27); IR (KBr) ν_{max}: 3397, 2924, 2852, 1641, 1314, 1289, 933 cm^{-1}; ^1H (500 MHz, $CDCl_3$) and ^{13}C NMR (125 MHz, $CDCl_3$), see Table 4, HR-ESI-MS *m/z* 337.1417 $[M + Na]^+$, (Calcd. for $C_{19}H_{22}NaO_4$, 337.1410).

*Isodon H (**8**).* Yellow powder; $[\alpha]_D^{25}$ −285.0 (*c* 0.131, MeOH); UV (MeOH) λ_{max} (log ε) 251.6 (4.32), 224.8 (4.09); ECD (MeOH) λmax 209.5 (+26.44), 246.5 (+34.18), 296.5 (−37.43); IR (KBr) ν_{max}: 3439, 2924, 2962, 1658, 1450, 1306, 1136, 752 cm^{-1}; ^1H (500 MHz, $CDCl_3$) and ^{13}C NMR (125 MHz, $CDCl_3$), see Table 4, HR-ESI-MS *m/z* 351.1936 $[M + Na]^+$, (Calcd. for $C_{21}H_{28}NaO_3$, 351.1931).

*4.4. X-ray crystallographic data for compounds **1**, **2**, **3**, and **6***

Crystals of compounds **1**, **2**, **3**, and **6** were obtained from $CHCl_3$–MeOH (2∶1) solutions. The crystallographic data for compounds **1, 2, 3**, and **6** were deposited in the Cambridge Crystallographic Data Centre (CCDC) with deposition numbers CCDC 2323446, CCDC 2323444, CCDC 2323445, and CCDC 2323447, respectively.

*Crystallographic data for isodon A (**1**)*: $C_{20}H_{26}O_4$ (*Mr* = 330.41 $g{\cdot}mol^{-1}$): orthorhombic, space group $P2_12_12_1$ (no. 19), *a* = 10.5904(2) Å, *b* = 10.7987(2) Å, *c* = 14.6254(3) Å, *V* = 1672.60(6) $Å^3$, *Z* = 4, *T* = 100 K, μ(Cu Kα) = 0.725 mm^{-1}, D_{calc} = 1.312 $g{\cdot}cm^{-3}$, 14841 reflections measured (10.182° ≤ 2θ ≤ 148.902°), 3395 unique (R_{int} = 0.0610, R_{sigma} = 0.0560) which were used in all calculations. The final R_1 was 0.0410 ($I > 2\sigma(I)$) and wR_2 was 0.1074 (all data). The goodness of fit on F^2 was 1.062. Flack parameter = −0.10(7).

*Crystallographic data for isodon B (**2**)*: $C_{20}H_{26}O_3$ (*Mr* = 314.41 $g{\cdot}mol^{-1}$): orthorhombic, space group Pbca (no. 61), *a* = 10.0039(2) Å, *b* = 11.9379(3) Å, *c* = 27.0983(7) Å, *V* = 3236.23(13) $Å^3$, *Z* = 8, *T* = 100.00 K, μ(Cu Kα) = 0.674 mm^{-1}, D_{calc} = 1.291 $g{\cdot}cm^{-3}$, 23618 reflections measured (6.524° ≤ 2θ ≤ 149.174°), 3279 unique (R_{int} = 0.0714, R_{sigma} = 0.0416) which were used in all calculations. The final *R*1 was 0.0560 ($I > 2\sigma(I)$) and w*R*2 was 0.1645 (all data). The goodness of fit on F^2 was 1.075.

*Crystallographic data for isodon C (**3**)*: $C_{20}H_{24}O_4$ (*Mr* = 328.39 $g{\cdot}mol^{-1}$): monoclinic, space group $P2_1/n$ (no. 14), *a* = 11.6683(4) Å, *b* = 6.7740(2) Å, *c* = 22.2248(8) Å, *β* = 94.351(2), *V* = 1751.61(10) $Å^3$, *Z* = 4, *T* = 100 K, μ(Cu Kα) = 0.692 mm^{-1}, D_{calc} = 1.245 $g{\cdot}cm^{-3}$, 17518 reflections measured (8.31° ≤ 2θ ≤ 148.776°), 3544 unique (R_{int} = 0.0805, R_{sigma} = 0.0549) which were used in all calculations. The final R_1 was 0.0526 ($I > 2\sigma(I)$) and wR_2 was 0.1407 (all data). The goodness of fit on F^2 was 1.069.

*Crystallographic data for isodon F (**6**)*: $C_{19}H_{22}O_3$ (*Mr* = 298.36 $g{\cdot}mol^{-1}$): orthorhombic, space group $P2_12_12_1$ (no. 19), *a* = 6.3850(2) Å, *b* = 6.9844(3) Å, *c* = 34.0215(12) Å, *V* = 1517. 20(10) $Å^3$, *Z* = 4, *T* = 100 K, μ(Cu Kα) = 0.695 mm^{-1}, D_{calc} = 1.306 $g{\cdot}cm^{-3}$, 33583 reflections measured (5.194° ≤ 2θ ≤ 149.728), 3104 unique (R_{int} = 0.0804, R_{sigma} = 0.0332) which were used in all calculations. The final R_1 was 0.0390 ($I > 2\sigma(I)$) and wR_2 was 0.0984 (all data). The goodness of fit on F^2 was 1.041. Flack parameter = −0.11(10).

4.5. Computational methods

The methodological details of ECD calculations are provided in the Supporting Information.

4.6. Cell culture

HepG2, L02, and AML12 cells (obtained from the Cell Bank of the Chinese Academy of Sciences, Shanghai, China) were cultured in DMEM supplemented with 10% FBS and 1% penicillin-streptomycin at 37 °C under conditions of 5% CO_2 and 95% humidity.

4.7. Luciferase reporter assay

HepG2 cells were transfected with pGL4.20-CYP7A1-Luc plasmids. Following 24 h of transfection, drug-containing medium was introduced after cell adherence in 96-well plates. After 24 h of drug exposure, the cells were lysed and analyzed for luciferase activity using a Duo-Lite™ Luciferase Assay System (Vazyme). Subsequently, the luciferase activity of drug-treated wells was compared with DMSO control wells.

4.8. Cytotoxicity assay

The cytotoxicity of the compounds was evaluated in AML12 cells using the CCK8 assay. AML12 cells were seeded in 96-well plates at a density of 1×10^4 cells per well and cultured for 24 h. Various concentrations of compounds (**1**–**21**) were administered to each well. After 24 h, 10 μL of CCK8 (10 $mg{\cdot}mL^{-1}$) was added to each well. The plate was then incubated for 24 h. Absorbance measurements at 450 nm were performed using an enzyme labeler (Molecular Devices, USA).

4.9. Animal treatments

Male C57BL/6J mice (obtained from Vital River, Beijing) were maintained in a temperature-controlled environment with unrestricted access to food and water, and housed on a 12 h light-dark cycle. Following 7 days of acclimatization, thirty male C57BL/6J mice (20 g ± 2 g, 7–8 weeks) were randomly allocated into six groups of four mice per group: control group, ANIT model group, ANIT + UDCA (100 $mg{\cdot}kg^{-1}$) group, ANIT + **6** (25 $mg{\cdot}kg^{-1}$) group, and ANIT + **6** (50 $mg{\cdot}kg^{-1}$) group. All groups received 10 $mL{\cdot}kg^{-1}$ corn oil as a solvent carrier by gavage for 5 consecutive days. On day 4, the control group received olive oil alone at 10 $mL{\cdot}kg^{-1}$, while other groups received ANIT (80 $mg{\cdot}kg^{-1}$) dissolved in olive oil by gavage. All mice were euthanized 48 h after ANIT administration. Blood and liver samples were collected in liquid nitrogen and stored at −80 °C. All animal experimental procedures were approved by the Animal Use and Ethics Committee of China Pharmaceutical University (No. 2023-10-008).

4.10. Biochemical analysis

Serum was obtained by centrifugation of blood samples after

1 h of standing. The levels of AST, ALT, ALP, and TBA were measured using commercial assay kits (Nanjing Jiancheng Bioengineering Institute), according to the manufacturer's protocol.

4.11. H&E, CK19, F4/80, and Sirius Red staining

Liver tissues fixed in 4% paraformaldehyde solution underwent wax block production and HE staining at the Pathology and PDX Pharmacodynamic Evaluation, China Pharmaceutical University. CK19, F4/80, and Sirius Red staining were performed at Wuhan Sevier Biotechnology Co.. Sections were scanned using a Nano Zoomer 2.0 RS slice scanner and analyzed using NDP software.

4.12. QRT-PCR analysis

Following the manufacturer's protocol, RNA was isolated from mouse liver tissues using the RNA-Quick Purification Kit (ES Science, Shanghai). HiScript® II Q Select RT SuperMix was utilized to reverse transcribe 1 μg total RNA into cDNA. QRT-PCR was conducted using SYBR Green reagent (Vazyme). The PCR primer sequences are listed in Table S1.

4.13. Western blotting analysis

Lysis buffer (CST, #9803S) containing protease inhibitor (MCE, IN) was used to lyse L02 cells, AML12 cells, and liver tissues. Protein concentrations were determined by BCA assay. Equal protein samples were separated by 8% SDS-PAGE gel and transferred onto PVDF membranes. The membranes were incubated with primary antibody overnight at 4 °C. After washing with TBST, the membranes were incubated with secondary antibodies. Table S2 lists the antibodies used in the study. Signals were detected using the LumiGLO chemiluminescent substrate system (TransGen Biotech, Beijing, China). Protein expression was analyzed using Image-Lab, with anti-β-actin as an internal reference.

4.14. Statistical analysis

Statistical differences between groups were analyzed using GraphPad Prism version 8.0.1 and the Student's *t*-test. All experimental values are expressed as mean ± SD. Results with $P < 0.05$ were considered statistically significant.

Funding

This work was supported by the National Key R&D Program of China (No. 2023YFD1601400), Jiangsu Outstanding Youth Fund Project (No. BK20231535), the National Natural Science Foundation of China (Nos. 82074068 and 82430118), the Basic Research Project for the Development of Modern Industrial College of Traditional Chinese Medicine and Health at Lishui University, Specialized Research Funds from the State Key Laboratory of Natural Medicines, China Pharmaceutical University (SKLNMZZ2024JS25), and the 111 Project (No. B18056).

Supplementary data

Supplementary data for this paper is available upon email request to the corresponding authors.

Declaration of competing interest

All authors declare that they have no conflict of interest.

References

1 Wu W, Li K, Ran X, et al. Combination of resveratrol and luteolin ameliorates α-naphthylisothiocyanate-induced cholestasis by regulating the bile acid homeostasis and suppressing oxidative stress. *Food Funct*. 2022;13(13):7098-7111. https://doi.org/10.1039/D2FO00521B.
2 Gao XG, Fu T, Wang CY, et al. Yangonin protects against cholestasis and hepatotoxity *via* activation of farnesoid X receptor *in vivo* and *in vitro*. *Toxicol Appl Pharmacol*. 2018;348:105-116. https://doi.org/10.1016/j.taap.2018.04.015.
3 Zheng SH, Cao PC, Yin ZQ, et al. Apigenin protects mice against 3,5-diethoxycarbonyl-1,4-dihydrocollidine-induced cholestasis. *Food Funct*. 2021;12(5):2323-2334. https://doi.org/10.1039/D0FO02910F.
4 Li T, Xu L, Zheng R, et al. Picroside II protects against cholestatic liver injury possibly through activation of farnesoid X receptor. *Phytomedicine*. 2019;68:153153. https://doi.org/10.1016/j.phymed.2019.153153.
5 Zhang S, Yu M, Guo F, et al. Rosiglitazone alleviates intrahepatic cholestasis induced by α-naphthylisothiocyanate in mice: The role of circulating 15-deoxy-$\Delta^{12,14}$-PGJ2 and Nogo. *Br J Pharmacol*. 2020;177(5):1041-1060. https://doi.org/10.1111/bph.14886.
6 Luo Z, Yin F, Wang X, et al. Progress in approved drugs from natural product resources. *Chin J Nat Med*. 2024;22(3):195-211. https://doi.org/10.1016/S1875-5364(24)60582-0.
7 Zhou W, Xie H, Wu P, et al. Abietane diterpenoids from *Isodon lophanthoides* var. *graciliflorus* and their cytotoxicity. *Food Chem*. 2012;136(2):1110-1116. https://doi.org/10.1016/j.foodchem.2012.08.015.
8 Wan J, Jiang HY, Tang JW, et al. *ent*-Abietanoids isolated from *Isodon serra*. *Molecules*. 2017;22(2):309. https://doi.org/10.3390/molecules22020309.
9 Lin L, Gao Q, Cui C, et al. Isolation and identification of *ent*-kaurane-type diterpenoids from *Rabdosia serra* (MAXIM.) HARA leaf and their inhibitory activities against HepG-2, MCF-7, and HL-60 cell lines. *Food Chem*. 2011;131(3):1009-1014. https://doi.org/10.1016/j.foodchem.2011.09.105.
10 Zhou W, Xie H, Xu X, et al. Phenolic constituents from *Isodon lophanthoides* var. *graciliflorus* and their antioxidant and antibacterial activities. *J Funct Foods*. 2013;6:492-498. https://doi.org/10.1016/j.jff.2013.11.015.
11 Liang Y, Xie H, Wu P, et al. Podocarpane, isopimarane, and abietane diterpenoids from *Isodon lophanthoides* var. *graciliflorus*. *Food Chem*. 2012;136(3-4):1177-1182. https://doi.org/10.1016/j.foodchem.2012.09.084.
12 Liu M, Wang WG, Sun HD, et al. Diterpenoids from *Isodon* species: an update. *Nat Prod Rep*. 2017;34(9):1090-1140. https://doi.org/10.1039/C7NP00027H.
13 Sun HD, Huang SX, Han QB. Diterpenoids from *Isodon* species and their biological activities. *Nat Prod Rep*. 2006;23(5):673-698. https://doi.org/10.1039/b604174d.
14 Lin CZ, Zhao W, Feng XL, et al. Cytotoxic diterpenoids from *Rabdosia lophanthoides* var. *gerardianus*. *Fitoterapia*. 2015;109:14-19. https://doi.org/10.1016/j.fitote.2015.11.015.
15 Tu WC, Huang YX, Li B, et al. Wulfenioidins D–N, structurally diverse diterpenoids with anti-Zika virus activity isolated from *Orthosiphon wulfenioides*. *J Nat Prod*. 2023;86(10):2348-2359. https://doi.org/10.1021/acs.jnatprod.3c00543.
16 Chen X, Liao RN, Xie QL. Abietane diterpenes from *Rabdosia serra* (maxim) hara. *J Chem Res*. 2001;39(32):200139197. https://doi.org/10.1002/chin.200139197.
17 Grandolini G, Casinovi CG, Betto P, et al. A sesquiterpene lactone from *Artemisia arborescens*. *Phytochemistry*. 1988;27(11):3670-3672. https://doi.org/10.1016/0031-9422(88)80792-1.
18 Zheng X, Kadir A, Zheng G, et al. Antiproliferative abietane quinone diterpenoids from the roots of *Salvia deserta*. *Bioorg Chem*. 2020;104:104261. https://doi.org/10.1016/j.bioorg.2020.104261.
19 Zhao A, Li S, Li Y, et al. Two new abietane quinones from *Isodon lophanthoides* var. *micranthus*. *Chin Chem Lett*. 2003;14(06):591-593. https://doi.org/10.1002/ciuz.200300280.
20 Jonathan LT, Che CT, Pezzuto JM, et al. 7-*O*-Methylhorminone and other cytotoxic diterpene quinones from *Lepechinia bullata*. *J Nat Prod*. 1989;52(3):571-575. https://doi.org/10.1021/np50063a016.
21 Eghtesadi F, Moridi Farimani M, Hazeri N, et al. Abietane and nor-abitane diterpenoids from the roots of *Salvia rhytidea*. *Springerplus*. 2016;5:1068. https://doi.org/10.1186/s40064-016-2652-0.
22 Yang F, Wang Y, Li G, et al. Effects of corilagin on alleviating cholestasis *via* farnesoid X receptor-associated pathways *in vitro* and *in vivo*. *Br J Pharmacol*. 2018;175(5):810-829. https://doi.org/10.1111/bph.14126.
23 Chambers KF, Day PE, Aboufarrag HT, et al. Polyphenol effects on cholesterol metabolism *via* bile acid biosynthesis, CYP7A1: a review. *Nutrients*. 2019;11(11):2588. https://doi.org/10.3390/nu11112588.
24 Zhao Y, He X, Ma X, et al. Paeoniflorin ameliorates cholestasis *via* regulating hepatic transporters and suppressing inflammation in ANIT-fed rats. *Biomed Pharmacother*. 2017;89:61-68. https://doi.org/10.1016/j.biopha.2017.02.025.